Mon. Not. R. Astron. Soc. **288,** 572–584 (1997)

Seismology of the base of the solar convection zone

Sarbani Basu

Teoretisk Astrofysik Center, Danmarks Grundforskningsfond, Institut for Fysik og Astronomi, Aarhus Universitet, DK-8000 Aarhus C, Denmark

Accepted 1997 February 3. Received 1997 January 30; in original form 1996 December 4

ABSTRACT

The base of the solar convection zone is a region of transition not just for the temperature gradient, but also for the internal rotation of the Sun. The discontinuity in the derivatives of the sound speed at the base of the overshoot layer below the solar convection zone (CZ) introduces a characteristic oscillatory component in the frequencies of solar p modes as a function of the radial order *n*. The amplitude of this signal can be calibrated using a sequence of solar models constructed with varying extent of overshoot below the CZ base. Using observed solar oscillation frequencies, we find an improved upper limit of $0.05H_p$ on the extent of overshoot. This technique also allows us to probe the composition profile at the CZ base, and we find that solar models with a sharp change in the composition gradients at the base of the CZ are ruled out from this study. It thus appears that there is some turbulent mixing just below the base of the CZ. The base of the CZ is also the region where the solar rotation rate changes from differential rotation in the CZ to nearly solid-body rotation in the radiative interior. Using modes that have their lower turning points near the transition region, we show that this transition occurs below the CZ base at a radial distance of 0.7050 ± 0.0027 $R_\odot$ over a half width of 0.0098 ± 0.0026 $R_\odot$. We also find an upper limit of 0.3 MG on the toroidal magnetic field concentrated below the CZ base.

Key words: convection – Sun: interior – Sun: magnetic fields – Sun: oscillations – Sun: rotation.

1 INTRODUCTION

The base of the solar convection zone (CZ) is a region of transition for the temperature gradient and for the internal rotation rate of the Sun. This is also the region where the solar dynamo is believed to operate. Thus this is an interesting and important region to investigate.

The transition in the temperature gradient makes the CZ base an ideal region with which to study the hydrodynamic properties of the Sun – particularly the amount of convective overshoot. This is so mainly because there is no accepted model of convection, and overshoot does not occur naturally in the different formulations used to calculate convective flux in the solar model. All reasonable models of convection indicate that convective elements overshoot into the radiative zone: however, the extent of overshoot is still a matter of debate. Helioseismology provides a tool for probing the base of the CZ and hopefully constraining theories that describe overshoot.

The CZ base is also important in terms of the internal dynamics of the Sun. Helioseismology has established that a shear layer with strong gradients of angular velocity exists around the CZ base (cf. Brown et al. 1989; Thompson et al. 1996). This layer separates the CZ, which exhibits strong differential rotation, and the radiative zone, which rotates almost like a rigid body. This region is considered to be the most likely place for the solar dynamo (cf. Weiss 1994). The strong gradient in the rotation rate is also expected to produce turbulence which is likely to mix material just below the CZ (cf. Richard et al. 1996).

Any spherically symmetric localized, sharp feature or discontinuity in the Sun's internal structure leaves a definite signature on the solar p-mode frequencies. Gough (1990) showed that abrupt changes of this type contribute a characteristic oscillatory component to the frequencies $\nu_{n,\ell}$ of those modes that penetrate below the localized perturbation. The amplitude of the oscillations depends on the 'severity' of the discontinuity. In a standard solar model, the transition of the temperature gradient from adiabatic to radiative values at the base of the solar CZ gives rise to an oscillatory signal in the frequencies of all modes that penetrate below the base of the solar CZ. In the presence of overshoot, the temperature gradient is almost discontinuous and the jump across the base of the convection zone increases with the extent of overshoot, and hence the amplitude of the oscillations increases. The amplitude of this signal can be calibrated as a function of the extent of overshoot by constructing solar models with known extents of overshoot, and the extent of the overshoot layer in the Sun can thus be estimated. This approach has been followed by Monteiro, Christensen-Dalsgaard & Thompson (1994), Basu, Antia & Narasimha (1994) and Basu & Antia (1994a), but these attempts have yielded only an upper limit to

the extent of overshoot as the estimated value is consistent with no overshoot within the expected errors.

There have been investigations (Roxburgh & Vorontsov 1994) that appear to show that the amplitude of the signal is not a monotonic function of the extent of overshoot, when the extent is very small. These authors find that as the extent of overshoot is increased, the amplitude first decreases before ultimately increasing for larger overshoot. This would of course mean that if, as evidence already suggests, overshoot below the solar CZ is small, it would be difficult to determine it precisely. The analysis was redone in slightly more detail by Christensen-Dalsgaard, Monteiro & Thompson (1995). Their results are systematically shifted with respect to those of Roxburgh & Vorontsov (1994), although they too find a local minimum.

Since the above studies involve approximate expressions that are derived under various assumptions, in this work we attempt to test the dependence of the amplitude on the extent of overshoot by constructing a series of solar models with varying extent of overshoot. These calibration models are also used to estimate the extent of the overshoot layer in the Sun using recent data from the GONG project (Harvey et al. 1996). We have also improved the fitting procedure to reduce systematic errors, which are now important, since the data errors have been reduced considerably. Christensen-Dalsgaard et al. (1995) performed a similar exercise and did not find any minimum in the amplitude as a function of the extent of overshoot for the models they constructed.

It is now believed that gravitational settling of helium and heavy elements below the CZ plays an important role in determining solar structure (cf. Cox, Guzik & Kidman 1989; Christensen-Dalsgaard, Proffitt & Thompson 1993; Basu & Antia 1994b etc.). This produces a gradient in the composition profile at the base of the CZ. The measurement of the extent of overshoot is, unfortunately, affected by systematic errors arising from gradients in the composition profile (cf. Basu & Antia 1994a) at the base of the CZ. Although it confuses the measurement of overshoot, this signal can be used to test whether the abundance profiles that result from different treatments of diffusion are consistent with the observed frequencies, and whether we do indeed have any evidence for mixing below the CZ base.

Matter can be mixed below the CZ base by circulations that are set up due to intense shear, and helioseismic inversions do detect a shear region (the 'tachocline') where solar rotation rate changes from differential rotation in the outer regions to solid body like rotation in the interior. Whether the transition in rotation rate around the CZ base is discontinuous (cf. Goode et al. 1991) or merely very steep is a matter of debate. Inversions are unable to resolve this because of finite resolution (cf. Thompson 1991). In either case, the abrupt change in the rotation rate leaves an oscillatory signal in the splittings (cf. Gough 1993). We show in this paper that, in principle, using this signal it is possible to probe the nature of the tachocline. However, we find that the currently available data are not good enough to detect this oscillatory signal. Data on frequency splittings for modes in the CZ and those with turning points around the CZ base are however quite precise. We show how these modes can be used to determine the precise position of the tachocline and also its thickness by considering the difference in splittings between the Sun and models with known position and thickness of the tachocline. This difference is calibrated using the corresponding difference in splitting between models with different position and thickness of the tachocline. We also investigate whether the even-order splitting coefficients provide any constraints on the magnetic field near the base of the CZ.

The rest of the paper is organized as follows. In Section 2, we describe results on the extent of overshoot below the CZ base and investigate the nature of the abundance profiles. In Section 3, we describe how frequency splittings are used to determine the position and width of the tachocline. In Section 4, we briefly attempt to determine the possible presence of a concentrated magnetic field below the CZ base, while the conclusions from our work are presented in Section 5.

2 OVERSHOOT BELOW THE CONVECTION ZONE

The transition of the temperature gradient from the adiabatic to radiative values at the base of the solar CZ gives rise to an oscillatory signal in the frequencies of all modes that penetrate below the base of the solar CZ. The oscillatory signal in the frequencies is amplified by considering the 4th differences of the frequencies, i.e.,

$$\delta^4\nu_{n,\ell} = \nu_{n+2,\ell} - 4\nu_{n+1,\ell} + 6\nu_{n,\ell} - 4\nu_{n-1,\ell} + \nu_{n-2,\ell}. \tag{1}$$

This procedure also eliminates the dominant non-oscillatory trend of the mode frequencies as a function of the radial order n.

The predominant, low-frequency oscillation in this 4th difference is due to the helium ionization zone located around 0.98 $R_\odot$. This component is estimated simultaneously while fitting the higher frequency signal due to the CZ base. The form fitted to the CZ base signal is the same as that in Basu et al. (1994), and takes into account the ℓ and ν dependence of the amplitude of the signal, i.e.,

$$\begin{aligned}\delta^4\nu = {} & a_1 + a_2\nu + \frac{(a_3 + a_4 L)}{\nu^2} \\ & + \left(a_5 + \frac{a_6}{\nu_m^2} + \frac{a_7 L}{\nu_m^2} + \frac{a_8 L}{\nu_m^4}\right) \sin(2\nu_m\tau_\mathrm{a} + \psi_\mathrm{a}) \\ & + \left(b_1 + \frac{b_2}{\nu_n^2} + \frac{b_3 L}{\nu_n^2} + \frac{b_4 L}{\nu_n^4}\right) \sin(2\nu_n\tau_\mathrm{b} + \psi_\mathrm{b}),\end{aligned} \tag{2}$$

where

$$\begin{aligned} L &= \ell(\ell+1), \\ \nu_m &= \nu - \frac{\gamma_\mathrm{a} L}{2\tau_\mathrm{a}\nu}, \\ \nu_n &= \nu - \frac{\gamma_\mathrm{b} L}{2\tau_\mathrm{b}\nu}. \end{aligned} \tag{3}$$

The coefficients in this expression are determined by a least-squares fit to the 4th differences. The coefficients a_1–a_4 define the smooth part, while a_5–a_8, τ_a and ψ_a determine the contribution due to the He II ionization zone and the remaining terms determine the contribution from CZ base. The frequencies of the two components τ_a and τ_b are approximately the acoustic depths of the helium ionization zone and the base of the CZ respectively, but they also include a contribution from the frequency-dependent part of the phases ψ_a and ψ_b which is not taken into account explicitly.

The form of the fitted function takes into account the ℓ-dependence of the signal due to the helium ionization zone. This was neglected in the earlier works (Basu et al. 1994; Basu & Antia 1994a), and its inclusion should decrease systematic errors and hence improve the reliability of the results. Since the amplitude of the signal is a function of frequency, the average amplitude in the frequency range 2 to 3.5 mHz is determined, after eliminating the degree dependence of the amplitude.

We consider modes with degrees 5 to 20, i.e., those that penetrate below the base of the CZ. Low-degree modes are not used as they have significantly larger errors. The mode-set is also restricted to

the frequency range 2–3.5 mHz. The lower limit is dictated by the fact that the amplitude of the signal due to the helium ionization zone becomes too large at lower frequencies for the signal to be removed reliably. The upper limit is dictated by the fact that errors in observed frequencies increase at larger frequency.

We have used a number of different data sets of observed frequencies to study the systematic errors introduced by uncertainties in the observed frequencies. These data sets are as follows.

(1) Data from the Big Bear Solar Observatory (BBSO) (Libbrecht, Woodard & Kaufman 1990).

(2) Global Oscillation Network Group (GONG) month 5 (Hill et al. 1996).

(3) GONG frequencies obtained from the averaged spectra for months 4–7, referred to as average GONG4–7.

(4) GONG frequencies obtained from the concatenated spectra for months 4–7, referred to as concatenated GONG4–7.

(5) GONG frequencies obtained from the averaged spectra for months 4–10, referred to as GONG4–10.

It should be noted that all earlier work was carried out with BBSO data only. We include that to show the difference made by the new data. This should give an estimate of how sensitive our technique is to systematic errors in different observed data sets.

2.1 Models used

We have constructed a number of static solar models for this work. To calibrate the signal due to overshoot, we use a series of solar models. We use envelope models for this purpose as in that case we can construct models with specified CZ depth and chemical abundances. The models used to investigate the abundance profile are full models.

All models have been constructed using the OPAL equation of state (Rogers, Swenson & Iglesias 1996) and OPAL opacities (Rogers & Iglesias 1992; Iglesias & Rogers 1996). In some cases at low temperatures we have used the opacities from Kurucz (1991). These models have the observed surface Z/X of 0.0245 (cf. Grevesse & Noels 1993).

The models used for overshoot calibrations have a helium abundance of 0.246 (cf. Basu & Antia 1995) and a CZ depth of 0.287 $R_\odot$ (cf. Christensen-Dalsgaard, Gough & Thompson 1991; Basu & Antia 1997). These models do not incorporate the diffusion of helium or heavy elements. We have used 11 models, with overshoot of 0–0.5 H_p, where H_p is the pressure scaleheight. These models are called OV0.xx, 0.xx being the extent of overshoot in units of H_p. We have to restrict our mode set further while using these models. These models extend to a depth of 0.4 $R_\odot$, and thus we can use only those modes that have a lower turning point above this lower boundary. The overshoot region in all these models is assumed to be adiabatically stratified.

In order to study the effect of the abundance profiles on the signal from the base of the CZ, and to test whether they are consistent with helioseismic data, we have used another set of models. The abundance profiles in these models are those obtained by various treatments of diffusion and settling of helium and heavy elements. These profiles have been scaled to obtain the desired surface abundances in all cases. These models do not have any overshoot.

The abundance profiles, which are shown in Fig. 1 are as follows.

ND. The hydrogen and heavy element abundance profiles from the no-diffusion model of Bahcall & Pinsonneault (1992). Since there is no diffusion in these models, there is no gradient in the composition profile below the CZ.

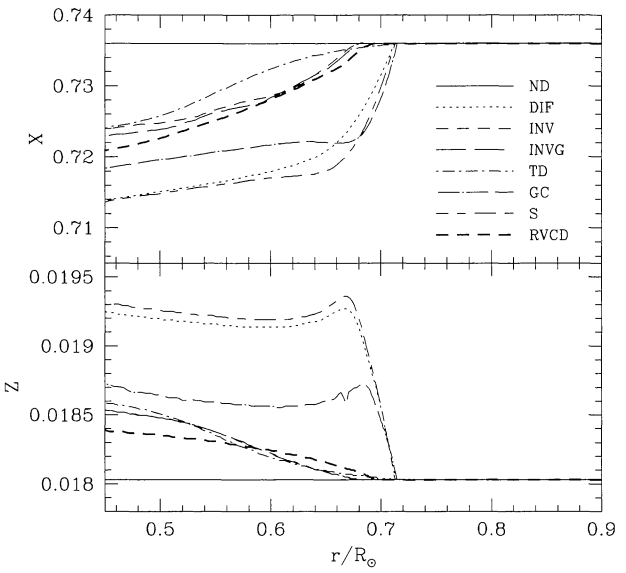

Figure 1. The abundance profiles in different solar models. The upper panel shows the hydrogen abundance profiles while the lower panel shows the Z profiles.

DIF. The hydrogen abundance profile incorporating the diffusion of helium from Bahcall & Pinsonneault (1992) and Z profile from Proffitt (1994). These profiles have a discontinuity in the gradient at the CZ base.

TD. The abundance profiles resulting from turbulent diffusion formulation TD2 of Christensen-Dalsgaard et al. (1993). Turbulence smoothes out the discontinuity at the CZ base and as a result, although an abundance gradient is still present, it is smooth.

GC. X and Z profiles from gradual mass-losing model 3b of Guzik & Cox (1995). Since their formulation of diffusion does not include turbulent mixing, the abundance profiles have a discontinuity in the gradient.

RVCD. X and Z profiles from model 5 of Richard et al. (1996). The model assumes rotation-induced mixing below the CZ base, hence the abundance profiles just below the CZ are very smooth and almost flat.

S. Model S of Christensen-Dalsgaard et al. (1996). In this case since the frequencies were also available we have used the original model and have not reconstructed it from the abundance profiles. The profiles are again very sharp, and the gradients are discontinuous at the base of the CZ.

INV. The hydrogen abundance profile obtained from helioseismic inversions (Antia & Chitre 1997) using the BBSO data, and a smoothed version of the Z profile from Proffitt (1994).

INVG. The hydrogen abundance profile obtained from helioseismic inversions using the GONG months 4–10 data.

12 models are used for this work. The models and their properties, like the surface abundances $Y_{\rm sur}$, $Z_{\rm sur}$, the position of the CZ base $r_{\rm b}$, etc., are summarized in Table 1.

2.2 Results

We first consider the variation of the mean amplitude of the signal with the extent of overshoot in a solar model and the results are shown in Fig. 2. Note that the increase in amplitude with extent of

Table 1. Solar models used.

Model	Type	X-profile	Z-profile	Y_{sur}	Z_{sur}	$r_b/R_\odot$	Low Temp. Opacity
NDF	Full	ND	ND	0.2645	0.01759	0.72696	OPAL
DIFF	Full	DIF	DIF	0.2479	0.01798	0.71641	OPAL
DIFE	Env.	DIF	DIF	0.2460	0.01803	0.71300	OPAL
INVF	Full	INV	INV	0.2444	0.01771	0.71342	OPAL
TD	Full	TD	ND	0.2472	0.01800	0.71459	OPAL
TDZ	Full	TD	TD	0.2518	0.01789	0.71734	OPAL
INVP	Full	INV	DIF	0.2485	0.01761	0.71412	OPAL
INVK	Full	INV	INV	0.2442	0.01771	0.71333	Kurucz
INVG	Full	INVG	INV	0.2452	0.01769	0.71341	Kurucz
GC	Full	GC	GC	0.2502	0.01793	0.71720	OPAL
RVCD	Full	RVCD	RVCD	0.2462	0.01803	0.71268	Kurucz
S	Full	S	S	0.2447	0.01806	0.71146	OPAL

overshoot is monotonic. We do not see any local minimum in the amplitudes for models that have overshoot between 0 and $0.1H_p$. This is contrary to the analytic expressions of Roxburgh & Vorontsov (1994) and Christensen-Dalsgaard et al. (1995). The difference is probably because of the approximations used in the analytic description. We do find a decrease in the slope of the amplitude–extent of overshoot relation for overshoot below $0.05H_p$. This could make determination of small overshoot somewhat difficult, but certainly not impossible, as would have been the case if there had been a minimum in the relation. We note that Christensen-Dalsgaard et al. (1995) also find the fitted amplitude to be monotonic.

The fits to the signal in the BBSO and GONG months 4–10 data are shown in Fig. 3. Note that the GONG data have a much cleaner signal – mainly because of smaller errors. This should, in principle, allow us to obtain a better limit to the extent of overshoot. The effect of data errors on the fitted parameters is found by Monte Carlo simulations, with 50 realizations of error for each data set. The simulations were carried out assuming that the mode errors have a Gaussian distribution with standard deviation given by the observational error of the mode. The average amplitude and frequency of the oscillatory signal for the different data sets and solar models are shown in Fig. 4, and the results are tabulated in Table 2. The amplitude gives a measure of the discontinuity, while the frequency of oscillations gives us a measure of the acoustic depth, τ_b, at which the discontinuity occurs. From the figure we see that the different observed data sets yield similar results and are consistent with each other within the estimated errors. A weighted average of all five observed data sets yields $A = 0.803 \pm 0.024$ μHz and $\tau = 2318.0 \pm 3.7$ s.

2.2.1 *Extent of overshoot*

Fig. 4 can be used to estimate the extent of overshoot in the Sun. Earlier estimates claimed 2σ upper limits of $(0.10–0.13)H_p$ (Basu et al. 1994; Monteiro et al. 1994; Basu & Antia 1994a; Christensen-Dalsgaard et al. 1995). From the figure we can see that because of improvement in data we are forced to revise downwards the earlier estimate and find an upper limit of $0.05H_p$. The improved data are also consistent with no overshoot and we can only give an upper limit. Note from the figure that there are some models that are not consistent with the observations despite having no overshoot: this is

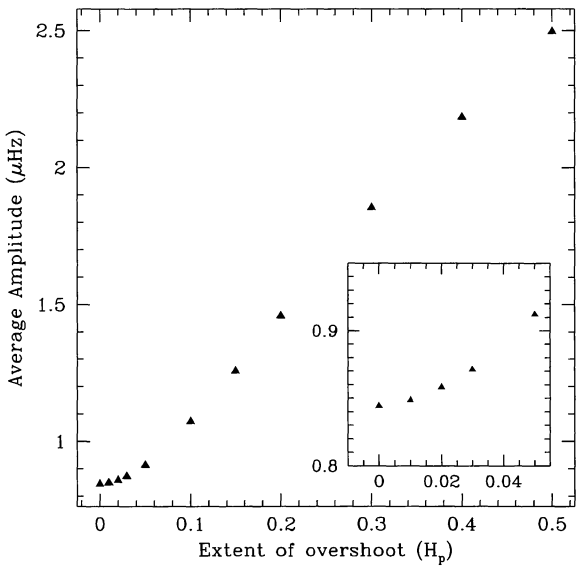

Figure 2. The amplitude of the signal plotted as a function of the extent of overshoot. Note that the amplitude increases monotonically with the extent of overshoot.

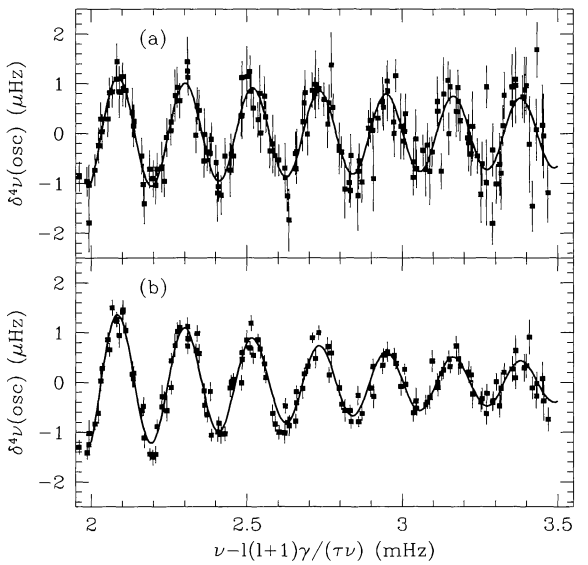

Figure 3. The fit to signal from the CZ base for (a) BBSO and (b) GONG months 4–10 data. The degree dependence of the differences has been removed from the points.

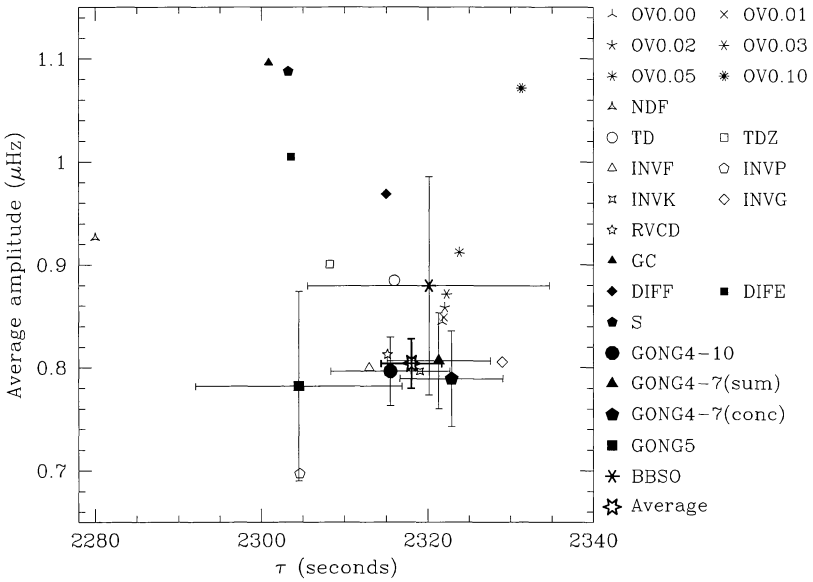

Figure 4. The amplitude A of the 4th differences plotted against the fitted acoustic depth τ for various test models. The points with the error bars are results using different observed frequencies.

caused by inconsistent abundance profiles and is discussed in the next subsection.

It may be noted that in this study we have assumed that the overshoot layer is adiabatically stratified. This is probably true in regions where the convective velocity is large enough to transmit significant convective flux, but if convective velocity becomes too small then the temperature gradient is likely to approach the radiative value and the resulting structure will not be different from the radiative layers, and it may not be possible to detect such layers helioseismically. Further, we are effectively assuming that the boundary layer where transition from adiabatic to radiative temperature gradient takes place is very thin.

Theoretical estimates of the extent of overshoot are rather uncertain as that requires a non-local theory of turbulence. Recently, such theories have become available (e.g., Canuto & Dubovikov 1996) that naturally lead to overshoot. Work currently in progress (Canuto et al., in preparation) seems to indicate that the extent of penetration is small and well within the helioseismic limits.

Table 2. Fitted amplitude and period of the CZ base signal.

Model	Amplitude μ Hz	τ_b seconds
OV0.00	0.844	2321.7
OV0.01	0.845	2321.9
OV0.02	0.858	2322.0
OV0.03	0.871	2322.3
OV0.05	0.912	2323.8
OV0.10	1.071	2331.3
OV0.15	1.258	2342.2
OV0.20	1.458	2354.8
OV0.30	1.853	2380.0
OV0.40	2.183	2403.7
OV0.50	2.496	2427.5
NDF	0.927	2280.0
DIFF	1.005	2303.6
DIFE	0.969	2315.0
GC	1.096	2300.9
S	1.088	2303.2
TD	0.885	2316.0
TDZ	0.900	2308.2
INVF	0.799	2312.9
INVP	0.697	2304.6
INVK	0.796	2319.0
INVG	0.805	2329.0
RVCD	0.813	2315.1
Observation		
BBSO	0.879 ± 0.106	2320.1 ± 14.6
GONG5	0.782 ± 0.092	2304.5 ± 12.4
GONG4–7 (concat)	0.789 ± 0.046	2322.9 ± 6.2
GONG4–7 (sum)	0.806 ± 0.046	2321.2 ± 6.2
GONG4-10	0.796 ± 0.033	2315.5 ± 7.2
Average	0.803 ± 0.024	2318.0 ± 3.7

2.2.2 *Abundance profiles*

From Fig. 4 we see that only models that have a smooth composition profile below the CZ base are consistent with observations. This is true even in the absence of any overshoot. This is due to the fact that the sudden increase in the mean molecular weight because of helium diffusion causes a decrease in the sound speed that adds to the contribution from change in the temperature gradient (Basu & Antia 1994a).

All models that have abundance profiles that are a result of non-turbulent diffusion appear to be ruled out from these results. In fact there is independent evidence from sound speed inversion results (Basu et al. 1996; Gough et al. 1996) that model S is inconsistent with helioseismic data just below the CZ. The Sun has a much higher sound speed in that region as compared with the model. The reason for this is probably that helium is less abundant in this region of the Sun than in the model. The amplitude of the oscillations gives an independent confirmation of this fact. Other models with a steep abundance gradient, like CG, are also inconsistent with observed frequencies.

The models with DIFF profiles that were marginally ruled out by the older BBSO data are clearly ruled out by the new data. Thus none of the models that have non-turbulent diffusion agrees with the

helioseismic data that are available now. The same is true for models TD and TDZ. Based on the older data sets, Basu & Antia (1994a) had concluded that turbulent diffusion of this type produces acceptable results. However, the new data force us to revise that conclusion.

The only models that seem to be consistent with the improved solar data in terms of both A and τ are INVF, INVK, INVG and RVCD. Although all these models have an abundance gradient at the base of the CZ, the profile is almost flat. Models INVF, INVK and INVG may be expected to match solar observations since the X-profile used was one obtained helioseismically. The fitted acoustic depth of INVF is, however, smaller than that of the observations. This is probably caused by low atmospheric opacities. The fact that INVK matches the observations is an indication of this. The fact that model RVCD is consistent with observations is encouraging: this indicates that there are physical processes that can be postulated to smooth out the abundance gradients by the right amount.

As for the models without any settling, the model OV0.0 has a consistent amplitude, but that is an envelope model. The full model with no diffusion (NDF) has a much higher amplitude, because of differences in X and the CZ depth. Besides, there is overwhelming evidence (see Basu 1997) that helium settling indeed takes place.

Thus it seems quite clear that models with a sharp gradient in their abundance profiles at the CZ base are not consistent with helioseismic data. There is, however, some uncertainty because of the Z-profile as can be seen from the results of model INVP. Unlike the X-profile, a rapid increase in Z causes the amplitude to decrease, because an increase in Z results in an increase in the opacity, which counteracts the reduction in temperature gradient. However, we have no reason to believe that heavy element diffusion will not be affected by turbulent mixing when helium diffusion is.

3 THE TRANSITION IN THE ROTATION RATE

Helioseismic inversions (e.g., Thompson et al. 1996) for rotation rate profile indicate a steep gradient around the base of the CZ where the rotation rate undergoes a transition from differential rotation in the CZ to essentially latitudinally independent rotation in the radiative interior. The resolution of these inversions is not sufficient to demonstrate whether the transition is discontinuous or merely steep. If the transition is discontinuous or takes place over length-scales much smaller than the vertical scales of p modes in that region, we can expect the splitting coefficients to show an oscillatory behaviour of the type studied above in the frequencies and this signal can again be calibrated. Another option is to look at those modes that have their turning points at the transition region. The effect of the tachocline will be the maximum for these modes (cf. Roxburgh & Vorontsov 1996). By calibrating this signal it should be possible to find out the position as well as the width of the tachocline.

3.1 The oscillatory signal in the splittings

We use the Ritzwoller & Lavely (1991) expansion of the rotation rate, where the rotation rate is expressed as

$$\Omega(r,\theta) = -\sum_{s=1,3,5,\ldots}^{\infty} \frac{\Omega_s(r)}{\sin\theta}\partial_\theta Y_s^0, \tag{4}$$

θ being the co-latitude, and the rotational splitting of the frequencies is written in terms of the splitting coefficients c_i such that

$$\delta\omega_{n\ell m} = \omega_{n\ell m} - \omega_{n\ell 0} = \sum_{s=1,3,5,\ldots} \gamma_{s\ell}^m c_s(n\ell), \tag{5}$$

where $\gamma_{s\ell}^m$s are known functions of m, s and ℓ, and c_s values, the splitting coefficients, are related to the rotation rates $\Omega_s(r)$.

Consider the splitting coefficient (see Ritzwoller & Lavely 1991)

$$c_3(n\ell) = \int_0^{R_\odot} \Omega_3 K_{n\ell}(r) r^2\, dr, \tag{6}$$

where the kernels

$$K_{n\ell}(r) = -\rho\frac{\xi_r^2 + \ell(\ell+1)\xi_h^2 - 2\xi_r\xi_h - 6\xi_h^2}{\int_0^{R_\odot}\rho(\xi_r^2 + \ell(\ell+1)\xi_h^2)r^2\, dr}, \tag{7}$$

ξ_r and ξ_h are respectively the vertical and horizontal components of displacement in the eigenvector for the corresponding mode, ρ is the density in the equilibrium solar model. Consider a simple model with rotation rate given by

$$\Omega_3(r) = \begin{cases} \Omega_0 & \text{if } r < r_d \\ \Omega_0 + \delta\Omega & \text{if } r \geq r_d \end{cases}. \tag{8}$$

Using the asymptotic approximation to describe the eigenfunctions, and neglecting the transverse component of the eigenfunctions (since we deal with low-degree modes which penetrate the CZ base) we can obtain an approximate expression of the form

$$c_3(n\ell) = c_{3s}(n\ell) + A(\ell,\omega)\cos(2\omega\tau - \beta/\omega + \psi), \tag{9}$$

where $c_{3s}(n\ell)$ is the smooth part of the splitting coefficient, τ is the acoustic depth of the position of the transition layer, and β is an ℓ-dependent coefficient. As in the case of the oscillations in the frequencies, this signal too can be amplified by taking the 4th difference of the splitting coefficients. The expression for the other splitting coefficients will be similar since the transverse components of the eigenfunctions have been neglected.

The splitting coefficients c_1, c_3 and c_5 for the data from GONG months 4–10 have been plotted in Fig. 5. Since c_3 shows the strongest gradient below the CZ, we use this coefficient to investigate the transition in the rotation rate.

In order to check what the oscillatory signal looks like, and to calibrate the signal, we use a series of artificial data sets constructed with different rotation rates. For the models with a transition, we model the rotation rate profile as

$$\Omega_3(r) = \Omega_c + \frac{\delta\Omega}{1 + \exp[(r_d - r)/w]}, \tag{10}$$

where Ω_c is the value of Ω_3 in the deep interior, w is the half-width of the transition layer, and r_d is the mid-point of the transition region. Thus the rotation rate increases from a factor $1/(1+e)$ of its maximum value to the factor $1 - 1/(1+e)$ of its maximum value in the range $r = r_d - w$ to $r = r_d + w$. The change $\delta\Omega = \Omega_{sur} - \Omega_c$ is the difference between the surface rotation rate Ω_{sur} and the rotation rate in the interior. The difference is approximately 20 nHz and is determined to match the observed c_3 for modes with lower turning point in the CZ (see Fig. 5) and will depend on Ω_c. The models used are as follows.

(1) R1: with

$$\Omega_3 = 20 \text{ nHz}. \tag{11}$$

(2) R2: with

$$\Omega_3 = 20 r/R_\odot \text{ nHz}. \tag{12}$$

(3) R3: with rotation rate as given by equation (10), with $r_d = 0.713\ R_\odot$, $w = 0.05\ R_\odot$ and $\Omega_c = 0$.

(4) R4: same as R3, but with $w = 0$, i.e., a discontinuous transition at $r_d = 0.713\ R_\odot$.

Since frequency splittings have much larger errors than the frequencies we have only fitted for the amplitude, period and

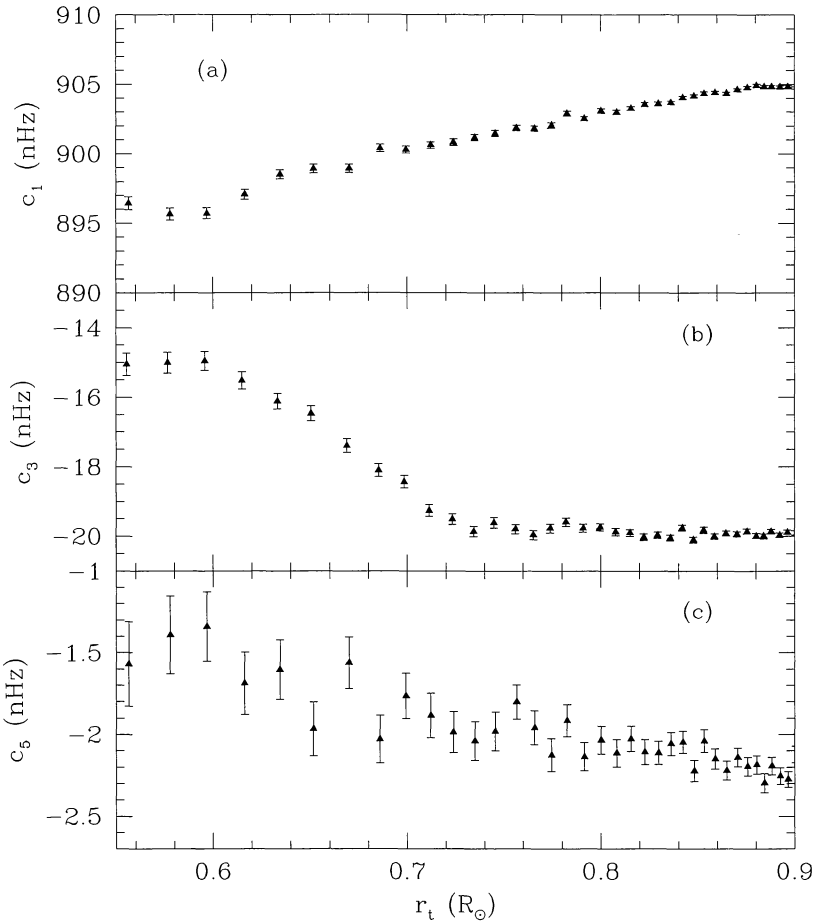

Figure 5. The splitting coefficients c_1, c_3 and c_5 obtained from the GONG4–10 data set. Each triangle is a weighted average over 15 modes. Only splittings of modes of degrees 6–150 in the frequency range 2 to 3.5 mHz have been used.

phase of the oscillatory trend in the 4th differences. The results of the fits are shown in Table 3. In Figs 6(a) and (b) we show the 4th differences for sets R3 and R4. We can see that in the case of a true discontinuity, the model has an amplitude much larger than one in which the same change occurs gradually. So in principle, the two cases are distinguishable. However, as can be seen from Fig. 6(c), the observations from the GONG4–10 set barely show any sign of oscillations, and the scale of variations is much larger than that of the models, despite the fact that the discontinuity in the models is equal to what is found from inversions. If we force a fit to a sinusoid, then the amplitude is much larger than any of the models. The reason is that the data errors are large and overwhelm the signal.

Table 3. Fitted parameters for 4th differences of the frequency splittings.

Model	Amplitude nHz	τ_b seconds
Exact splittings		
R1	0.00538	2099.7
R2	0.05276	2346.6
R3	0.13651	2359.1
R4	1.50662	2328.4
GONG4–10	12.508 ± 2.509	1871.2 ± 237.0
Monte-Carlo simulations		
R3		
Full errors	8.289 ± 2.519	1666.5 ± 215.1
Error/2	4.251 ± 1.219	1663.0 ± 212.7
Error/4	2.075 ± 0.631	1668.3 ± 217.6
R4		
Full errors	9.076 ± 2.531	1823.4 ± 237.0
Error/2	4.572 ± 1.272	1823.9 ± 234.0
Error/4	2.338 ± 0.640	1801.1 ± 234.5
Pure noise		
Full errors	9.030 ± 2.509	1757.0 ± 235.8
Error/2	4.527 ± 1.264	1826.9 ± 234.5
Error/4	2.278 ± 0.649	1826.0 ± 235.5

To check this we have added errors to the artificial data sets R3 and R4 from a normal distribution of errors, with the standard deviation of the distribution given by the observers' error estimates. The results for one realization of error each are shown in Figs 6(d) and (e). Note that the two sets look indistinguishable in the presence of errors. Thus with the present level of observational error, it is not possible to use this technique to infer whether the transition of the rotation rate is discontinuous or merely steep.

To check the level of uncertainty we have fitted for the amplitude and period for R3 and R4 after adding the errors with a normal distribution. The standard deviation of the error distribution was taken to be equal to the quoted errors in the GONG4–10 set. We repeated the exercise with standard deviation of half the quoted errors and a fourth of the quoted errors. For each level of errors we have used 20 realizations of error to find the mean amplitude and period, and also the spread in the values as given by the standard deviation of the distribution. To check whether the errors can give a spurious signal, we have just used the random errors without the underlying signal. The results of this exercise are also tabulated in

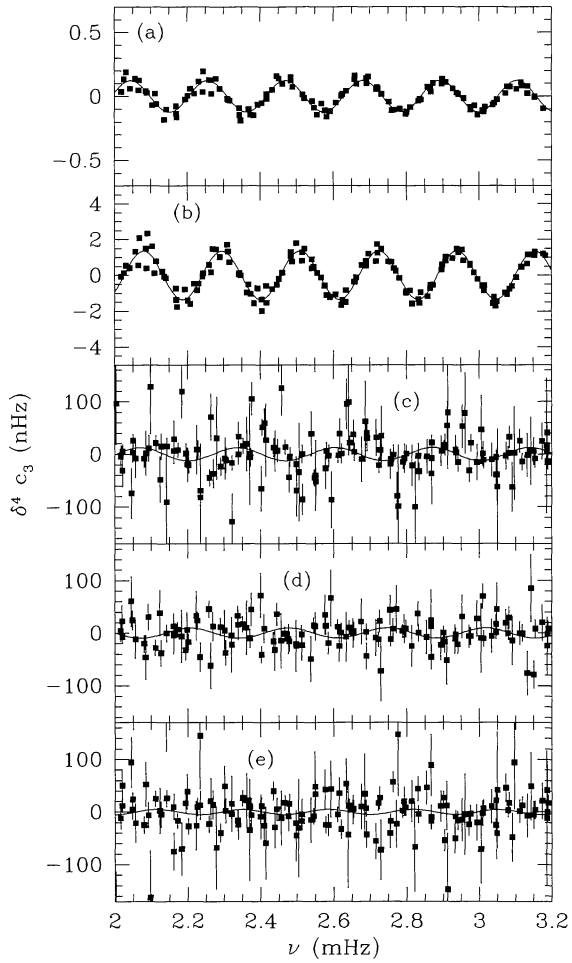

Figure 6. The 4th differences of the splittings in set (a) R3, (b) R4, (c) GONG4–10 observations, (d) R3 with errors added, and (e) R4 with errors added.

Table 3. Note that the amplitude of the signal for the models increases in the presence of errors and is of the same level as those for the GONG4–10 data. The results are disappointing since, even with a drastic reduction in the error level, it would be almost impossible to detect the signal. Just pure noise could produce a spurious signal with a similar amplitude and period to the observed set of splittings. Thus the observational errors need to be reduced by more than a factor of 4 for us to be able to detect any signal. Hence, for the present data sets, we have to use a different technique to determine the position and thickness of the transition layer. We discuss an alternative technique in the next subsection.

3.2 The position and thickness of the tachocline

The drawback of trying to fit the oscillatory signal in the splittings is that it relies on splittings of low-degree modes, and these have very large errors. By far the most precise data are for modes that have their turning points in the CZ. Reasonably reliable data are available for modes that sample up to a depth of about 0.6 $R_\odot$. These are the modes that should be used to determine the position and thickness of the tachocline.

If there is a perturbation in solar structure the modes that are most affected are those that have their turning points near the perturbation (cf. Roxburgh & Vorontsov 1996), similarly a sharp transition

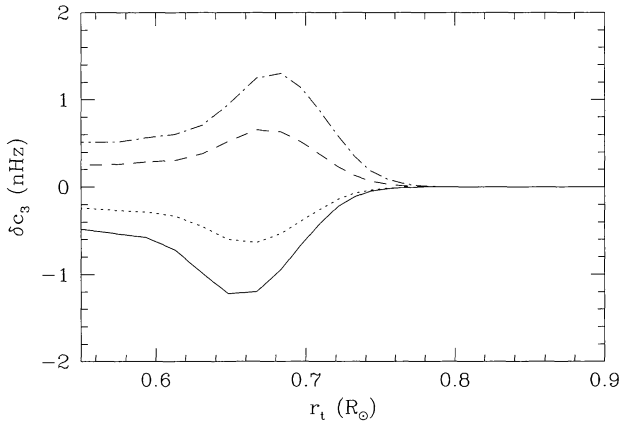

Figure 7. The difference in c_3 between the rotation models with discontinuity at 0.70 $R_\odot$ and those with discontinuity at 0.68 $R_\odot$ (continuous line), 0.69 $R_\odot$ (dotted line), 0.71 $R_\odot$ (dashed line) and 0.72 $R_\odot$ (dot-dashed line) plotted as a function of the lower turning point of the modes. For each model the splittings have been averaged in groups of 15 modes.

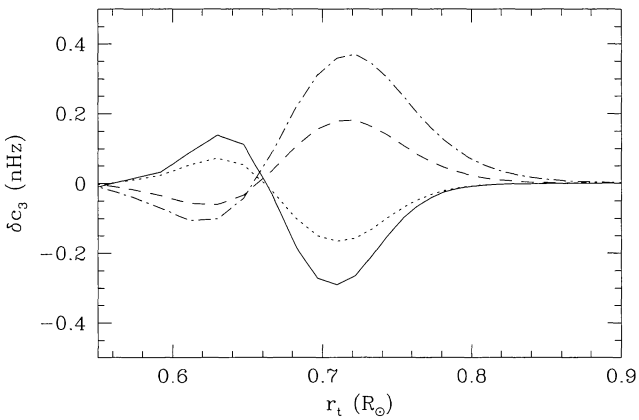

Figure 8. The difference in c_3 between the rotation model with $w = 0.015$ $R_\odot$ and those with $w = 0.005$ (continuous line), 0.01 (dotted line), 0.02 (dashed line) and 0.025 $R_\odot$ (dot-dashed line).

in rotation rate will have maximum effect on the splittings of those modes that have their turning points near the transition region (cf. Gough & Thompson 1990, hereafter GT). Since the transition in the solar rotation rate is known to be close to the CZ base, the splittings that are most affected are also the more reliably determined modes. Thus these modes should give a reliable estimate of the position and thickness of the transition region.

In Fig. 7 we show the difference in the splitting coefficients between similar models that have discontinuities at different positions. The difference is taken for the averaged splittings. Note that the differences are zero in the CZ, they have a well-defined peak and the height of the peak is proportional to the difference in the positions of the discontinuity. Thus the peak height can be calibrated to find the position of the discontinuity.

We can use a similar calibration to test the thickness over which the transition of the rotation rate occurs. In Fig. 8 we show the difference in splitting coefficients for rotation models with different widths of transition. The width of the peak in δc_3 between two models is proportional to the thickness of the wider transition, and a simple scaling of the radius around the peak position can reduce the curves to similar widths.

The models described above assume that Ω_3 in the deep interior, Ω_c, is zero. It may be possible to determine the interior value of Ω_3

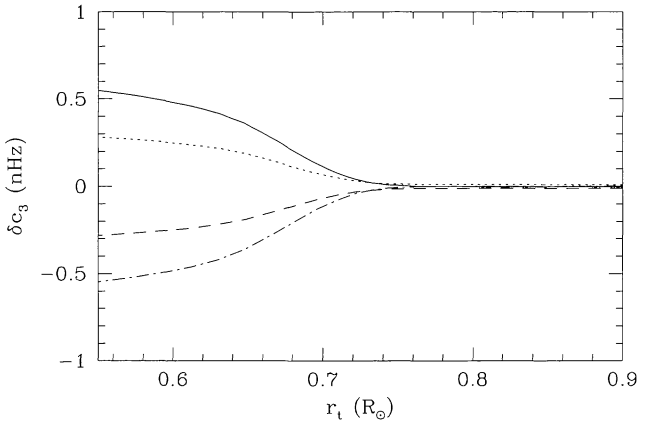

Figure 9. The difference in c_3 between a rotation model with an Ω_c of 0 and those with -2 (solid line), -1 (dotted line), 1 (dashed line) and 2 (dot-dashed line) nHz.

using a similar method of calibration. For this we use equation (10) with a non-zero Ω_c and $\delta\Omega$ is chosen so that for modes with turning points in the CZ the resultant c_3 matches the observations. A finite Ω_3 in the interior thus means a change in the effective amount of the discontinuity. Other attempts at investigating the tachocline (e.g., Kosovichev 1996) have not considered the possibility of a non-zero Ω_3 in the interior. In Fig. 9 we show the difference between models with $r_d = 0.705$ $R_\odot$ and $w = 0.005$ $R_\odot$, but with different values of Ω_c. Note, from the figure, that the difference in the coefficients does not show a peak, but merely a smooth step. Thus it could be more difficult to determine this quantity. Ideally r_d, w and Ω_c should be determined simultaneously, however, for simplicity in this work we determine these parameters by independent fits. Since statistical errors arising from uncertainties in observed splittings are found to dominate over the systematic errors, such a procedure may not introduce significant additional errors.

We, therefore, find that to determine the position and width of the transition all that needs to be done is to find the height of the peak (after scaling r with width in the case of thickness determination) in the difference between the observed coefficients and model coefficients and calibrate that against known models. To find Ω_c, the height of the step has to be calibrated. The procedure can be easily tested using some artificial test models. There would be some systematic errors in this procedure arising because of other differences between the calibration models and the test models. We find that if the model characteristics are very different, e.g., if the calibration models for finding r_d have a discontinuous jump and the test model has a finite transition width, or if the test model has a different Ω_3 in the interior from those of the calibration models, the difference in coefficients δc_3 has an additional component on which the peak is superimposed. However, we find that the smooth component can be modelled as a low-degree polynomial and removed. In the case of solar data additional systematic errors may arise because Ω_3 may not be constant in the CZ or in the interior as has been assumed. The rotation rate profile in the transition layer in the Sun may also be very different from that assumed in the models.

3.2.1 *The procedure*

For each of the tasks, i.e., determination of position of the tachocline, determination of the width of the tachocline and determination of Ω_3 in the interior, we have constructed a series of five calibration models with known properties. For the purpose of calibration, we consider δc_3 between neighbouring models and fit a spline through the points

$$\phi(r) = \delta c_3(r) = \sum_i a_i \psi_i(r), \tag{13}$$

where the $\phi(r)$s are the calibration curves and $\psi(r)$s are the cubic B-spline basis functions. Thus we have four calibration curves from the five calibration models. For convenience we follow a naming convention for the models. The models are called M*xx*d*yy*I*zz*, where 0.*xx* is $r_d/R_\odot$, *yy*/1000 is $w/R_\odot$ and *zz* is Ω_c in nHz. Thus, for determining r_d we use the calibration models M68d00I00, M69d00I00, M70d00I00, M71d00I00, M72d00I00, i.e., models with $r_d/R_\odot = 0.68, 0.69, 0.70, 0.71, 0.72$ with $w = 0$ and $\Omega_c = 0$, and differences in c_3 between the successive calibration models define the four calibration curves.

The difference in c_3 between each calibration model and the observations (or test model) can be fitted with the form

$$\delta c_3 = \alpha\phi(r) + f(r), \tag{14}$$

where $\phi(r)$ is the calibration curve defined above and $f(r)$ is a low-degree polynomial used to take into account systematic effects arising from differences in other parameters, like Ω_c, width, etc. between the observations (or test models) and the calibration models. Tests show that a polynomial of degree 2 is optimum for this purpose. A lower degree polynomial does not fit the smooth part too well, and the problem with a higher degree polynomial is that it may also fit a part of the real signal. Depending on the calibration curves used, α gives the difference between the position of transition, width of transition or Ω_c between the calibration curve and the Sun (or test model). The constant α and the coefficients of the polynomial $f(r)$ are obtained by a least-squares fit to the data. In practice, we determine α for all five calibration models and interpolate to find the points where $\alpha = 0$. The four calibration curves give four results which are then averaged.

In practice, α is determined by a fit in the fairly narrow range of 0.6 to 0.9 $R_\odot$ for the lower turning point. Although in principle Ω_c would be better determined by including modes with turning points at lower radii, the lower limit is dictated by the fact that data error becomes very large. The upper limit is chosen to avoid the effects of the shear layer known to exist just below the solar surface (cf. Thompson et al. 1996).

We have used three sets of data: splittings obtained from GONG months 4–7, GONG months 4–10 and the average of BBSO splittings (Woodard & Libbrecht 1993) for the years 1986–1990. It must be noted that the BBSO splittings are available only on a Legendre polynomial basis function – the so-called a-coefficients, which have been converted to the c coefficients using known transformations (cf. Ritzwoller & Lavely 1991). In order to determine the uncertainty in the results due to data errors, we have performed Monte Carlo simulations on models using the observers' error estimates.

To determine the position of discontinuity, the calibration models have been constructed using equation (10) with transitions at 0.68, 0.69, 0.70, 0.71 and 0.72 $R_\odot$, and $w = 0$. To determine the width over which the transition occurs, we have constructed a set of models using equation (10), with $r_d = 0.70$ $R_\odot$, and $w = 0.005$, 0.01, 0.015, 0.02 and 0.025 $R_\odot$. For convenience, the models are called M70d05I00–M70d25I00. In order to determine Ω_c, we have constructed models with $r_d = 0.705$ $R_\odot$, $w = 0.005$ $R_\odot$ and Ω_c of -2, -1, 0, 1 and 2 nHz. These models are called M705d05I–2–M705d05I+2. To test the method and study the systematic errors

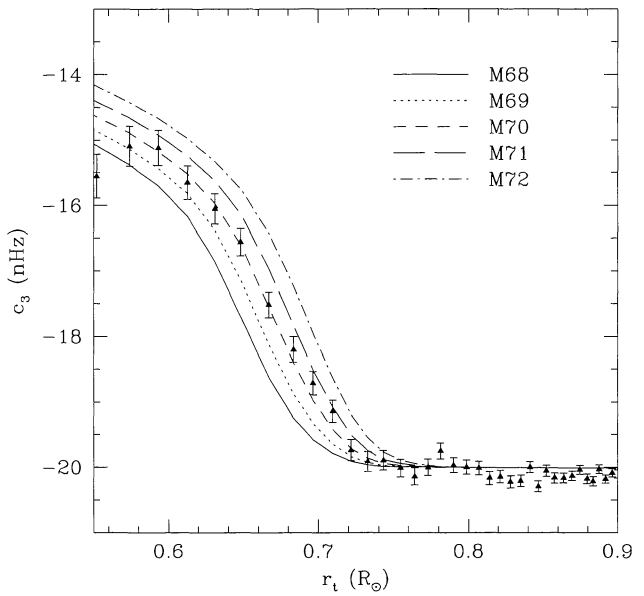

Figure 10. The coefficients c_3 for the GONG4–10 set plotted along with those of models M68d00I00–M72d00I00.

involved, we have used a number of test models with the same naming convention.

3.2.2 *Results*

The observed c_3 has been plotted with those of some of the calibration models in Fig. 10. Note how well the models fit the observations: it is difficult to gauge the differences from the figure. The difference in c_3 between the different sets of calibration models and observation from the GONG4–10 set are shown in Fig. 11. Note that the differences are small. Just by inspection of the figures, it appears that r_d is between 0.70 and 0.71 $R_\odot$, i.e. below the base of the solar CZ which is seismically determined to be at 0.713 $R_\odot$ (Christensen-Dalsgaard et al. 1991; Basu & Antia 1997). The half-thickness appears to be quite small, less than 0.015 $R_\odot$. The signal for Ω_3 in the interior is, however, not clear. The detailed results from the fits are shown in Table 4. Table 4 also lists the results for some of the test models used. The models listed give an indication of the systematic errors involved, which are discussed later in this section.

As far as the position of the transition is concerned, the results bear out what can be seen in the figure: transition in the solar rotation rate occurs below the base of the solar CZ. All three sets of data give very similar results. The error in the determination of r_d due to errors in the data is less than 1 per cent.

To check the magnitude of possible systematic errors, one has to look at the results obtained for the test models. If the test and calibration models are similar, then we find that the position of the transition can be determined very accurately. There are definite systematic errors if the test model has a finite thickness of transition, or a non-zero Ω_3 in the interior. A finite thickness causes r_d to be overestimated, while a finite Ω_c causes it to be underestimated slightly. Results for test models, including those listed in Table 4, indicate a maximum systematic error of about 0.0015 $R_\odot$. This error is only about one-quarter of that due to data errors in the GONG4–7 set and less than half the error due to data errors in the GONG4–10 set, hence, we can claim that the position of the tachocline can be determined quite robustly. A weighted average

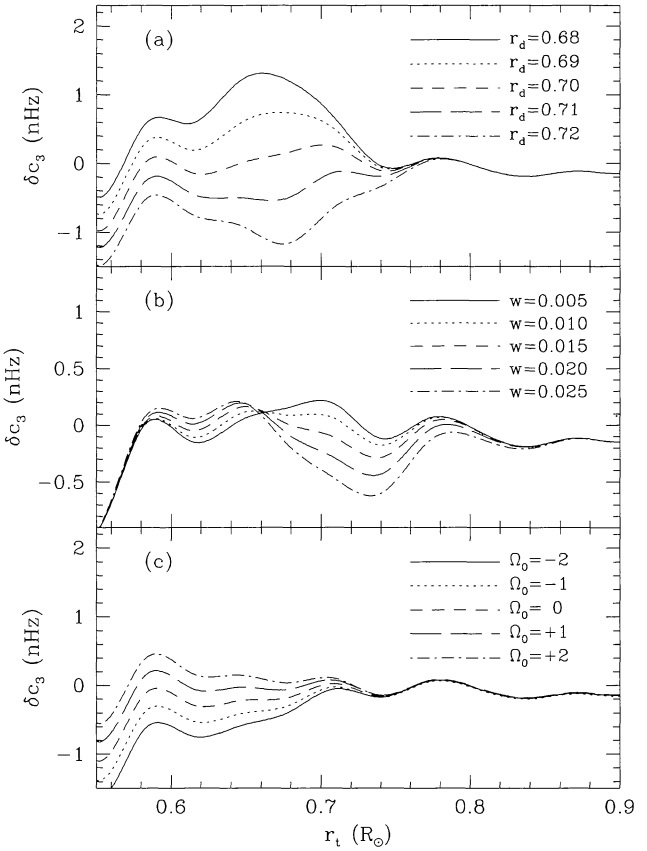

Figure 11. The least-squares fit through δc_3 between different calibration models and observation from the GONG4–10 set. Panel (a) shows differences with calibration models for r_d, panel (b) with w calibration models, and panel (c) with Ω_c calibration models.

of the three data sets implies that the mid-point of the transition is at 0.7050 ± 0.0027 $R_\odot$.

All three data sets give similar results for the thickness of the transition too. The statistical uncertainties are, however, larger, and so are the systematic errors due to differences between the test models and the calibration models. However, in this case the systematic errors are almost comparable to the statistical uncertainties. Assuming that the error in the position of the tachocline is what is obtained in the previous exercise, the maximum expected systematic error is less than 0.0020 $R_\odot$ from the results for several test models. A weighted mean of results for the three data sets is 0.0098 ± 0.0026 $R_\odot$.

The value of r_d determined above is different from that obtained by Kosovichev (1996). Using models with transitions at different positions and by determining the minimum of the χ^2 between the BBSO data and the models, Kosovichev (1996) finds the transition to be centred at 0.692 ± 0.005 $R_\odot$. However, using constrained forward modelling techniques, and a completely different data set, Charbonneau et al. (1997) have obtained results similar to ours, i.e., $r_d = 0.704 \pm 0.003$ $R_\odot$.

Our results on the thickness of transition are apparently very different from those of the others. For instance Kosovichev (1996) obtains 0.09 ± 0.04 $R_\odot$, while Charbonneau et al. (1997) obtain 0.050 ± 0.012 $R_\odot$. The difference, however, arises due to the definition of the thickness. They have used a rotation model

$$\Omega_3 = \delta\Omega 0.5\left\{1 + \mathrm{erf}\left[2\frac{(r - r_d)}{w}\right]\right\}. \quad (15)$$

Table 4. Results about the tachocline.

Determining r_d Model/Obs.	Exact value $R_\odot$	Estimated value $R_\odot$
M70d00I00	0.7000	0.6992
M705d00I00	0.7050	0.7052
M70d10I+2	0.7000	0.7012
M705d10I00	0.7050	0.7064
M705d00I+2	0.7050	0.7049
BBSO	–	0.7066 ± 0.0047
GONG4–7	–	0.7034 ± 0.0056
GONG4–10	–	0.7048 ± 0.0039
Average	–	0.7050 ± 0.0027
Determining w Model/Obs.	**Exact value $R_\odot$**	**Estimated value $R_\odot$**
M70d01I00	0.0100	0.0101
M70d13I00	0.0133	0.0132
M705d10I00	0.0100	0.0126
M70d10I+2	0.0100	0.0119
M705d10I+2	0.0100	0.0142
BBSO	–	0.0084 ± 0.0053
GONG4–7	–	0.0100 ± 0.0050
GONG4–10	–	0.0105 ± 0.0036
Average	–	0.0098 ± 0.0026
Determining Ω_c Model/Obs.	**Exact value nHz**	**Estimated value nHz**
M705d05I+.5	0.500	0.5093
M705d05I+2.25	2.250	2.2468
M705d10I00	0.000	2.7702
M70d10I00	0.000	3.3997
BBSO	–	-2.0351 ± 5.7877
GONG4–7	–	1.2898 ± 5.4558
GONG4–10	–	2.1487 ± 3.0267
Average	–	0.8663 ± 2.5321

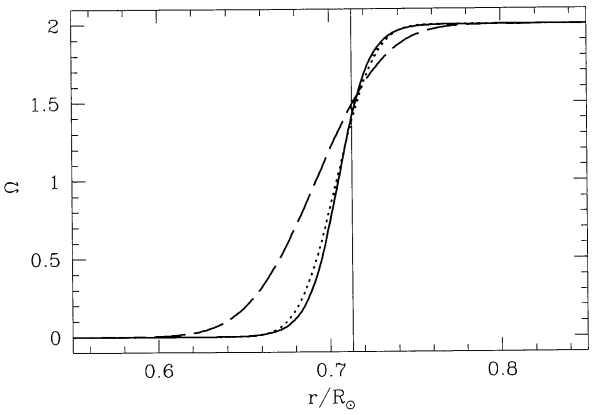

Figure 12. The profile of the rotation rate in the tachocline. The continuous curve is the one obtained using weighted averages of parameters obtained in this work (but with $\Omega_c = 0$), the dotted curve is that obtained by Charbonneau et al. (1997) and the dashed curve is that obtained by Kosovichev (1996). The amplitude has been assumed to be 1 at $r = r_d$. The vertical line denotes the position of the CZ base.

The thickness w represents the variation of Ω_3 from 0.08 to 0.92 of $\delta\Omega$. The width defined by us is half the width of the variation of Ω_3 from 0.269 to 0.731 of its value. We have plotted the Ω_3 profile obtained using the parameters calculated by us along with those from Kosovichev (1996) and Charbonneau et al. (1997) in Fig. 12. Note the remarkable agreement between our results and those of Charbonneau et al. These results were obtained using completely different methods as well as observed data, and hence increase our confidence in the numbers obtained. Note, however, that the errors on the determination of thickness are quite large and the result is consistent with a discontinuous transition at the 4σ level.

The results obtained for Ω_c are, however, not very robust. We can see from Table 4 that reliable results can be obtained only if the test and calibration models are similar. The three sets of observed data give three different results, and, within errors, they are consistent with zero. Because the calibration method does not provide us with a reliable result we have considered a series of models with $r_d = 0.705$ and $w = 0.01$ and tried to find out the value of Ω_c for which a minimum χ^2 is obtained. The three sets of data give us slightly different results. The BBSO data give a minimum at about $\Omega_c = 0.5$ nHz, while GONG4–7 and GONG4–10 have a minimum for $\Omega_c = 2.5$ nHz. However, the uncertainties are roughly same as those shown in Table 4. So these results are within 1σ of what was found by fitting. If $\Omega_3 = 0$ in the interior, the rotation rate would be independent of latitude. Our results tend to suggest that $\Omega_c = 0$ is not inconsistent with the data. Further, we can put a 1σ upper limit of about 3 nHz on Ω_c.

4 MAGNETIC FIELD AT THE CZ BASE

Solar dynamo theories place the solar dynamo at the base of the CZ, where the rotation rate shows strong gradients (e.g., Weiss 1994). The field is believed to be accumulated in this thin layer. If the layer were to extend too deeply into the CZ, the field would be destroyed by convection. Using techniques very similar to those used to study overshoot and the transition in the rotation rate, we attempt to put a limit on the magnetic field. Earlier results of Goode & Dziembowski (1993) put a limit of 1 MG for the toroidal magnetic field below the solar CZ base.

Just like rotation, magnetic fields break the spherical symmetry of the Sun and thus cause frequency splittings. Unlike rotation these splittings can be expanded in even powers of the azimuthal quantum number m (cf. Gough 1993) and can be written as

$$\Delta\omega_{n\ell m} = \sum_{\lambda=0}^{2k} Q_{\lambda\ell m} I_\lambda, \tag{16}$$

where $Q_{\lambda\ell m}$ are known functions and I_λ is the splitting coefficient.

GT demonstrated that a toroidal magnetic field concentrated in a thin layer introduces an oscillatory signal in the even-order splittings of modes that penetrate the layer. The amplitude of the oscillations is about 20 μHz for the splitting coefficient I_2 and about 7.5 μHz for I_4 with a 10-MG magnetic field located around the base of the CZ. The splitting coefficients I_2 and I_4 can be obtained from the Legendre polynomial splitting coefficients a_2 and a_4, and hence for this work we use the GONG4–10 Legendre polynomial splitting coefficients. We do not correct for the second-order effects of rotation as that is unlikely to contribute an oscillatory signal of this magnitude.

In Fig. 13 we show the 4th difference of the splittings I_2 and I_4 for the GONG4–10 data. Also shown are fits to the oscillatory function. The amplitudes obtained are 0.184 ± 0.057 μHz for I_2 and 0.487 ± 0.185 μHz for I_4. The results are at the 3σ level, but like

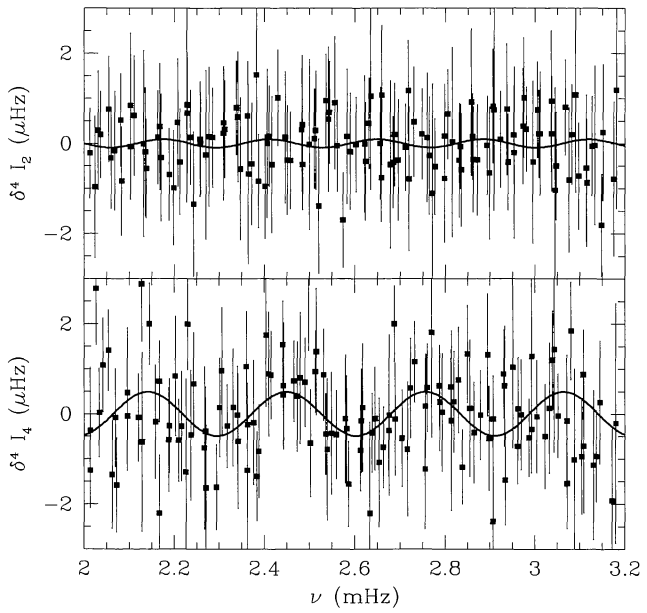

Figure 13. The 4th difference of splittings I_2 and I_4 in the GONG4–10 set. The continuous line is the fit to a sinusoidal function.

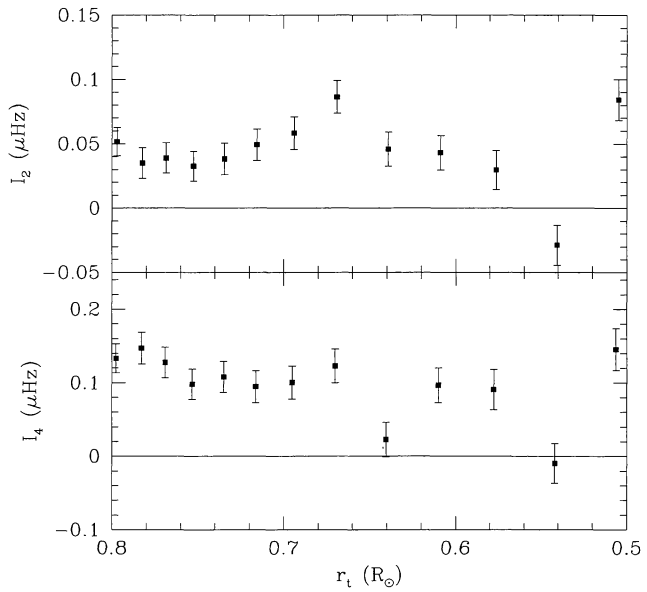

Figure 14. Splitting coefficients I_2 and I_4 of the GONG4–10 set plotted against the lower turning point. The data have been averaged over groups of 25 modes.

in the case of rotational splittings, may not be significant. To check this we find the amplitude for 25 realizations of error, assuming that the exact splittings are zero. We thus try to find the signal in the case of pure noise. The mean amplitudes obtained were 0.24 for I_2 and 0.43 for I_4. However, if we assume that the amplitude is actually due to magnetic field, we can put an upper limit on the magnetic field. From Section 3.1 we have seen that a decrease in error will cause a decrease in the fitted amplitude, thereby decreasing the estimate on the magnetic field. Thus this value should be considered to be an upper limit.

From artificial data on rotational splittings we find that the amplitude of oscillations in the 4th difference of the splittings is about a factor of 10 greater than those in the plain splittings. Adopting the same factor here, we obtain amplitudes of 0.0184 and 0.0497 μHz for I_2 and I_4, respectively. It may be noted that since this factor mainly depends on the acoustic depth of the tachocline it is expected to be similar for all the splitting coefficients. Comparing these amplitudes with those obtained by GT, and noting that the amplitude varies as the square of the magnetic field, we obtain fields of 0.30 MG from I_2 and 0.81 MG from I_4, i.e. the upper limit is less than that obtained by Goode & Dziembowski (1993).

Since the above method only gives us an upper limit, we look at the splittings as a function of their lower turning points. GT have shown that modes that have a turning point around the layer with the field are affected most, and when plotted as a function of r_t, the lower turning point, they show a distinct peak. For a field of 10 MG, I_2 has a peak of about 80 μHz and I_4 about 60 μHz for $\ell = 40$.

We have plotted the splittings from the GONG4–10 in Fig. 14 after averaging them in groups of 25 modes. We can see that while I_2 appears to show a peak, for I_4 the situation is not clear. We find the peak amplitude by considering the difference between the lowest and highest points in the range 0.6–0.75 $R_\odot$. The mean ℓ of the modes that contribute to the splittings in this region is about 40 and hence we can directly compare with the peak height as determined by GT, which again scales as the square of the field. The amplitude of the I_2 signal is 0.046 ± 0.010 μHz, where the error estimate is obtained by a Monte Carlo simulation. For each realization of error the data were averaged and the peak height determined in the manner explained above. The error mentioned is the standard deviation of the set of amplitudes obtained from the exercise. The amplitude of I_2 corresponds to $B = 0.24 \pm 0.03$ MG. Averaging over 15 instead of 25 points increases the peak amplitude, but the errors are larger too.

To check the significance of these results, we have repeated the above exercise with pure noise of the same magnitude as the observed errors in I_2. The average height of the peaks between 0.6 and 0.75 $R_\odot$ is 0.023 nHz, for I_2. This value is roughly half of what is obtained for the observations, and is slightly more than 2σ lower. Thus the observations appear to be significant at the 2σ level and there does seem to be some hint of a magnetic field slightly lower than the upper limit obtained from the oscillations. The signal in I_2 is somewhat clearer, so it is possible that the field in the Sun is about 0.2 MG. This result is again much lower than the limit of 1 MG set by Goode & Dziembowski (1993) and is consistent with the limit as estimated by Gough et al. (1996).

From Fig. 14 we see that there is a 2σ signal in I_2, while the situation for I_4 is not so clear. We thus use only I_2 to put the upper limit on the magnetic fields near the CZ base, and as seen above we obtain an upper limit of 0.3 MG. The reason that I_4 does not give any conclusive result could be because of the much larger errors present. However, it is possible that the field configuration in the Sun may be different from what GT have considered and hence I_2 and I_4 give different results. It is of course possible that the signal in the coefficients is not due to magnetic fields at all, but asphericity in the shape of the CZ base. The asphericity would be of order I_2/ν, which is approximately 10^{-5}.

5 CONCLUSIONS

We have made a thorough investigation of the structure and dynamics of the solar CZ base using available helioseismic data. We have used the frequencies to study the extent of overshoot below the base of the solar CZ and study the abundance gradients in that region. We have used the frequency splittings to determine the

position and width of the tachocline. We have also used the even frequency splitting coefficients to put limits on possible toroidal magnetic fields confined to a thin layer below the CZ base.

We find that the use of new data and better fitting techniques allow us to put an improved upper limit of $0.05H_p$ (2800 km) on the extent of overshoot below the solar CZ. This estimate is lower than those obtained earlier. However, like earlier results this estimate is also based on the assumption that the overshoot region is adiabatically stratified. The signal used to determine the overshoot can be used to probe the abundance gradient at the CZ base, and we find that models that have abundance profiles that do not allow for any mixing just below the base of the CZ are not consistent with the observations. Only models where the abundance profile is smoothed out, for instance by rotationally induced mixing, are consistent. Such mixing could also explain the low lithium abundance in the solar envelope.

Mixing due to rotation requires the presence of a strong shear region. Rotation inversions have shown the existence of a shear layer around the base of the solar CZ where the rotation rate changes from being latitudinally dependent to almost solid body like. In this work we find that the layer in which this transition takes place is situated at a radial distance of 0.7050 ± 0.0027 $R_\odot$, a little below the base of the solar CZ, and has a half width of 0.0098 ± 0.0026 $R_\odot$, the width being defined as the region where the rotation rate increases from 0.269 to 0.731 of its maximum value. The layer is thus very narrow, however with the adopted form of the transition, the upper part of the transition region penetrates into the CZ. Thus, if the transition in the Sun does have a similar form, it could cause the mixing needed to smooth out the abundance profiles. We can also put a 1σ upper limit of 3 nHz on Ω_3 in the interior.

The shear layer at the base of the solar CZ is also believed to be the region where the toroidal magnetic fields associated with the solar dynamo reside. We put an upper limit of 0.3 MG on the magnetic field from the splitting coefficient I_2. This limit is lower than the limits placed earlier. A field of this magnitude is too small to affect the structure of the Sun significantly and, in particular, to affect the estimates of the extent of the overshoot region. The magnetic field will have to be a few MG to have a noticeable effect on the results (cf. Basu et al. 1994).

ACKNOWLEDGMENTS

The author thanks Joyce Guzik, Olivier Richard and Jørgen Christensen-Dalsgaard for sending their solar models. This work was supported by the Danish National Research Foundation through its establishment of the Theoretical Astrophysics Center. This work utilizes data obtained by the Global Oscillation Network Group (GONG) project, managed by the National Solar Observatory, a Division of the National Optical Astronomy Observatories, which is operated by AURA, Inc., under a cooperative agreement with the National Science Foundation.

REFERENCES

Antia H. M., Chitre S. M., 1997, submitted
Bahcall J. N., Pinsonneault M. H., 1992, Rev. Mod. Phys., 64, 885
Basu S., 1997, in Provost J., Schmider F. -X., eds, Proc. IAU Symp. 181, Sounding Solar and Stellar Interiors. Kluwer, Dordrecht, in press
Basu S., Antia H. M., 1994a, MNRAS, 269, 1137
Basu S., Antia H. M., 1994b, JA&A, 15, 143
Basu S., Antia H. M., 1995, MNRAS, 276, 1402
Basu S., Antia H. M., 1997, MNRAS, in press
Basu S., Antia H. M., Narasimha D., 1994, MNRAS, 267, 209
Basu S., Christensen-Dalsgaard J., Schou J., Thompson M. J., Tomczyk S., 1996, ApJ, 460, 1064
Brown T. M., Christensen-Dalsgaard J., Dziembowski W. A., Goode P. R., Gough D. O., Morrow C. A., 1989, ApJ, 343, 526
Canuto V. M., Dubovikov M. S., 1996, Phys. Fluids, 8, 12
Charbonneau P., Christensen-Dalsgaard J., Henning R., Schou J., Thompson M. J., Tomczyk S., 1997, in Provost J., Schmider F. -X., eds, Proc. IAU Symp. 181, Sounding Solar and Stellar Interiors, Posters Volume. Kluwer, Dordrecht, in press
Christensen-Dalsgaard J., Gough D. O., Thompson M. J., 1991, ApJ, 378, 413
Christensen-Dalsgaard J., Proffitt C. R., Thompson M. J., 1993, ApJ, 408, L75
Christensen-Dalsgaard J., Monteiro M. J. P. F. G., Thompson M. J., 1995, MNRAS, 276, 283
Christensen-Dalsgaard J. et al., 1996, Sci, 272, 1286
Cox A. N., Guzik J. A., Kidman R. B., 1989, ApJ, 342, 1187
Goode P. R., Dziembowski W. A., 1993, in Brown T. M., ed., GONG 1992, Seismic Investigation of the Sun and Stars. ASPCS, 42, 229
Goode P. R., Dziembowski W. A., Korzennik S. G., Rhodes E. J., 1991, ApJ, 367, 649
Gough D. O., 1990, in Osaki Y., Shibahashi H., eds, Lecture Notes in Physics, 367. Springer, Berlin, p. 283
Gough D. O., 1993, in Zahn J. -P., Zinn-Justin J., eds, Astrophysical Fluid Dynamics, Les Houches Session XLVII. Elsevier
Gough D. O., Thompson M. J., 1990, MNRAS, 242, 25 (GT)
Gough D. O. et al., 1996, Sci, 272, 1296
Grevesse N., Noels A., 1993, in Prantzos N., Vangioni-Flam E., Cassé M., eds, Origin and evolution of the Elements. Cambridge Univ. Press, Cambridge, p. 15
Guzik J. A., Cox A. N., 1995, ApJ, 448, 905
Harvey J. W. et al., 1996, Sci, 272, 1284
Hill F. et al., 1996, Sci, 272, 1292
Iglesias C. A., Rogers F. J., 1996, ApJ, 464, 943
Kosovichev A. G., 1996, ApJ, 469, L61
Kurucz, R. L., 1991, in Crivellari L., Hubeny I., Hummer D. G., eds, Proc. NATO ASI Series, Stellar atmospheres: beyond classical models. Kluwer, Dordrecht, p. 441
Libbrecht K. G., Woodard M. F., Kaufman J. M., 1990, ApJS, 74, 1129
Monteiro M. J. P. F. G., Christensen-Dalsgaard J., Thompson M. J., 1994, A&A, 283, 247
Proffit C. R., 1994, ApJ, 425, 849
Richard O., Vauclair S., Charbonnel C., Dziembowski W. A., 1996, A&A, 312, 1000
Ritzwoller M. H., Lavely E. M., 1991, ApJ, 369, 557
Rogers F. J., Iglesias C. A., 1992, ApJS, 79, 507
Rogers F. J., Swenson F. J., Iglesias C. A., 1996, ApJ, 456, 902
Roxburgh I. W., Vorontsov S. V., 1994, MNRAS, 267, 297
Roxburgh I. W., Vorontsov S. V., 1996, MNRAS, 278, 940
Thompson M. J., 1991, Sol. Phys., 125, 1
Thompson M. J. et al., 1996, Sci, 272, 1300
Weiss N. O., 1994 in Proctor M. R. E, Gilbert A. D., eds, Lectures on Solar and Planetary Dynamo. Cambridge Univ. Press, p. 59
Woodard M. F., Libbrecht K. G., 1993, ApJ, 402, L77

This paper has been typeset from a TEX/LATEX file prepared by the author.